Plasmonic silver nanosphere enhanced ZnSe nanoribbon/Si heterojunction optoelectronic devices

2016 Nanotechnology 27 215202

(http://iopscience.iop.org/0957-4484/27/21/215202)

IOP Publishing Nanotechnology
Nanotechnology 27 (2016) 215202 (9pp) doi:10.1088/0957-4484/27/21/215202

Plasmonic silver nanosphere enhanced ZnSe nanoribbon/Si heterojunction optoelectronic devices

Li Wang, Ran Chen, Zhi-Fei Ren, Cai-Wang Ge, Zhen-Xing Liu, Shu-Juan He, Yong-Qiang Yu, Chun-Yan Wu and Lin-Bao Luo

School of Electronic Science and Applied Physics and Anhui Provincial Key Laboratory of Advanced Materials and Devices, Hefei University of Technology, Hefei, Anhui 230009, People's Republic of China

E-mail: luolb@hfut.edu.cn

Received 1 February 2016, revised 6 March 2016
Accepted for publication 16 March 2016
Published 15 April 2016

Abstract

In this study, we report a localized surface plasmon resonance (LSPR) enhanced optoelectronic device based on a ZnSe:Sb nanoribbon (NR)/Si nano-heterojunction. We experimentally demonstrated that the LSPR peaks of plasmonic Ag nanoparticles (Ag NPs) can be readily tuned by changing their size distribution. Optical analysis reveals that the absorption of ZnSe:Sb NRs was increased after the decoration of the Ag NPs with strong LSPR. Further analysis of the optoelectronic device confirmed the device performance can be promoted: for example, the short-circuit photocurrent density of the ZnSe/Si heterojunction solar cell was improved by 57.6% from 11.75 to 18.52 mA cm^{-2} compared to that without Ag NPs. Meanwhile, the responsivity and detectivity of the ZnSe:Sb NRs/Si heterojunction device increased from 117.2 to 184.8 mA W^{-1}, and from 5.86×10^{11} to 9.20×10^{11} cm $Hz^{1/2}$ W^{-1}, respectively.

Keywords: zinc selenide, localized surface plasmon resonance, solar cell, photodetector, optoelectronic devices

(Some figures may appear in colour only in the online journal)

Introduction

One of the main obstacles for the efficiency enhancement of optoelectronic devices is the conflict between the need for a thick absorption layer to ensure sufficient photon absorption while maintaining a thin film to achieve a short exciton diffusion length. Noble metal nanoparticles (NPs) with localized surface plasmon resonance (LSPR) have recently attracted wide attention for possible applications in solar cells [1–3], and photodetectors [4, 5], because they may greatly improve the light trapping ability without obviously increasing the physical thickness of the absorption layers [6–9]. This is especially important for nanstructure-based optoelectronic devices, which are normally composed of nanobelts [10], nanowires [11, 12] or nanoribbons (NRs) [13, 14], possessing the potential advantages of more efficient charge collection, and enhanced light trapping and absorption ability [15–17].

Nanometer-sized noble metal (gold (Au) [18] or silver (Ag) [19]) particles are interesting candidates in the above optoelectronic devices, as they possess a relatively strong scattering efficiency, a broad LSPR absorption band in the visible range, and high chemical stability [20]. For example, plasmonic Ag NPs have been widely used in various optoelectronic devices such as solar cells [21], water splitters [22], UV photodetectors [23], and light emitting diodes [24]. An extensive study has reported that the energy transfer between plasmonic NPs and the photoactive region of a solar cell may occur both via the strongly enhanced electromagnetic near field on the length scales of the particle dimensions, and via far-field effects [1]. In device applications [25, 26], it is vitally important to control the LSPR peak of metallic NPs to a target wavelength at which the best optical performance of the absorption layer materials can be obtained [27]. Up to now many strategies have been investigated to engineer LSPR properties such as tailoring the size, shape, arrangement, and

geometry of metal nanostructures, or the local dielectric environment [28]. To date, whilst considerable work has been carried out to optimize the optoelectronic devices using Au NPs, relatively little work has been studied to boost nano-optoelectronic devices using Ag NPs which are equally important plasmonic materials [29–31]. In this work, we report a high-performance plasmonic optoelectronic device based on a ZnSe NR/Si heterojunction by decorating Ag NPs with localized surface plasmon resonance. Our experimental result shows that the LSPR peak of Ag NPs can be readily tuned in the range of 411 to 429 nm only by changing the particle sizes. Further device analysis reveals that after decoration with Ag NPs, the short-circuit photocurrent density of the ZnSe NR/Si heterojunction solar cell is improved by 57.6% from 11.75 to 18.52 mA cm^{-2} compared to that without Ag NPs. What is more, the responsivity of the ZnSe NRs/Si heterojunction photodetector increases from 117.2 mA W^{-1} to 184.8 mA W^{-1} after modification with Ag NPs (39 + 64 nm), and its detectivity rises from 5.86 $\times$ 10^{11} to 9.20 $\times$ 10^{11} cm $Hz^{1/2}$ W^{-1}.

Experimental details

Synthesis and analysis

The *p*-type ZnSe NRs were synthesized with ZnSe and Sb powders in a horizontal alumina tube furnace via a conventional vapor–liquid–solid process. In a typical experiment, ZnSe powder (0.2 g) was first loaded into an alumina boat and transferred to the central region of the furnace. Another boat filled with 0.02 g Sb powder was then placed at the upstream position. Silicon substrate coated with 10 nm Au catalyst was placed at the downstream 10 cm from the ZnSe source. The reaction chamber was filled with a gas mixture of 20 sccm Ar and H_2 (5% in volume). The temperatures of the ZnSe powder, Sb powder and silicon substrate were maintained at 1000, 900, and 700 °C, respectively, during the experiment. After growth for 2 h, the system was cooled down to room temperature and the Si substrate was covered with a layer of yellow wool-like product. The Ag NPs were prepared by a modified method in a round bottom flask, in which $AgNO_3$ and citrate solution ($C_6H_5Na_3O_7 \cdot 2H_2O$) were used as precursors. In this experiment, Ag NPs were synthesized by the classic Lee–Meisel method in a vessel. First, 1.7 ml of 1% $AgNO_3$ aqueous solution was added to a 100 ml of water in a three-necked round bottom flask and the mixture was brought to boiling by an oil bath for 15 min. Next, 2 ml of 1% citrate solution was added to the reaction solution. The reaction solution was kept under vigorous mechanical stirring for 1 h. After reaction, the three-necked round bottom flask was opened and cooled to ambient conditions. For the Ag NPs dispersion, an ethanol solution containing Ag NPs was drop-cast onto the ZnSe NRs. The ZnSe NRs were then heated at 60 °C for rapid evaporation of ethanol to prevent the aggregation of Ag NPs. The morphologies and structures of the as-synthesized ZnSe NRs and Ag NPs were characterized by field-emission scanning electron microscopy (FESEM, Sirion 200 FEG), high-resolution transmission electron microscopy (HRTEM, JEOL-2010), and x-ray diffraction (XRD, D-500 using Cu Ka radiation). The chemical compositions of the NRs were analyzed by x-ray photoelectron spectroscopy (XPS, Thermo ESCALAB 250). Absorption spectra were determined on a Varian UV-Cary 100 spectrophotometer. To construct the ZnSe NR/Si p-n nano-heterojunction, as-synthesized p-ZnSe NRs were transferred onto a SiO_2 (300 nm)/n-Si substrate with patterned Si windows etched by a buffered oxide etch solution via a simple sliding transfer process. Part of the ZnSe NRs could contact the exposed n-Si within the patterned windows, forming the ZnSe NR/Si p-n heterojunctions. Afterwards, Cu (4 nm)/Au (45 nm) electrodes were deposited onto the part of the ZnSe NRs on SiO_2 film serving as Ohmic contacts to the NRs. All the electrical property measurements of the devices were carried out on a semiconductor characterization system (Keithley 4200-SCS).

Theoretical simulation

To simulate the LSPR effect of the Ag NPs, the finite element method (FEM) was used in this work. In the simulation, we only consider a unit cell of the models with a fixed period in an aqueous environment (n = 1.33). The sizes of the Ag NPs in the models were set to be identical to that obtained from the SEM images. In addition, the permittivity of Ag was obtained from the Sopra SA Company database. The perfect electric conductors and perfect magnetic conductors were employed for four lateral boundaries respectively. The perfectly matching layers were applied in the propagation directions to eliminate nonphysical boundary reflections. The transverse magnetic polarized light was assumed to be normally incident from the top of the structure and a stationary solver was built to solve the different frequency light coupling effect with plasmonic nanostructures.

Results and discussion

In this study, the Ag NPs were grown by an Ag seed assisted method, via which the size of Ag NPs can be readily tuned by using smaller size Ag NPs as seeds. Figures 1(a)–(c) display typical SEM images of the as-prepared Ag NPs. According to the size histogram shown in the insets in figures 1(a)–(c), the average diameters of the Ag NPs are 39 ± 2 nm, 48 ± 2 nm and 64 ± 2.5 nm, respectively. Further XRD analysis reveals that these Ag NPs are of cubic phase (figure 1(d)). The high-solution TEM image showed that the lattice spacing is 0.24 nm, which is in agreement with Ag (111) planes (2.36 Å) (figure 1(e)). To study the optical property of the Ag NPs, we then studied the UV–vis absorption spectrum in the range from 360–510 nm. As shown in figure 1(f), all the Ag NPs with different sizes exhibit obvious absorption peaks at approximately 400 nm in the absorption spectrum. Understandably, the intensive absorption band at about 400 nm can be ascribed to the LSPR band which is due to the strong interaction between the electric field of the incident electromagnetic radiation and the particle's electrons [32]. This

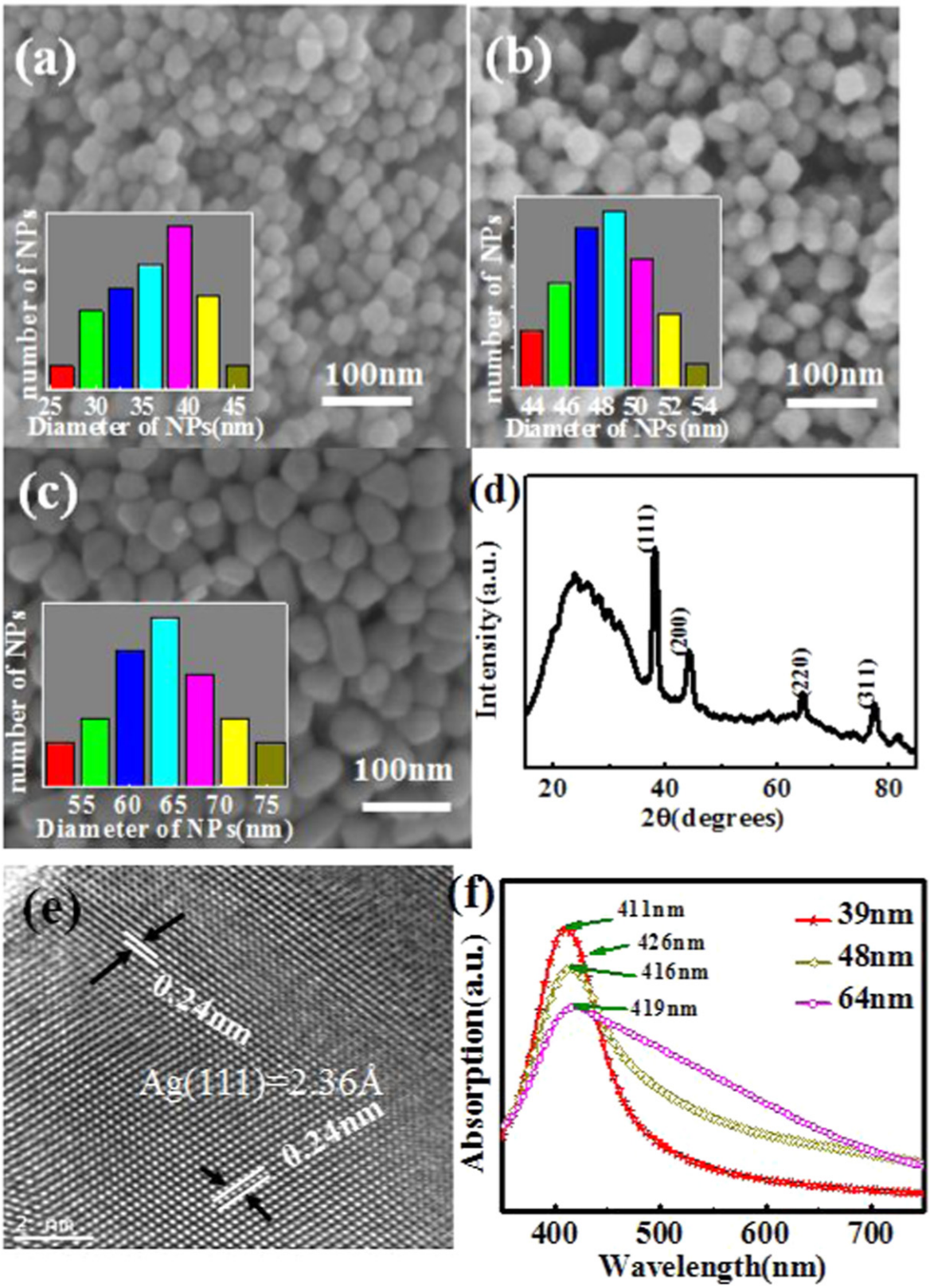

Figure 1. (a)–(c) SEM images of Ag NPs (39 ± 2 nm, 48 ± 2 nm, 64 ± 2.5 nm); the inserts are the corresponding size distribution diagrams of Ag NPs. (d) XRD pattern of the Ag NPs. (e) HRTEM image of the Ag NPs. (f) Absorption curves of Ag NPs with different sizes (39 ± 2 nm, 48 ± 2 nm, 64 ± 2.5 nm).

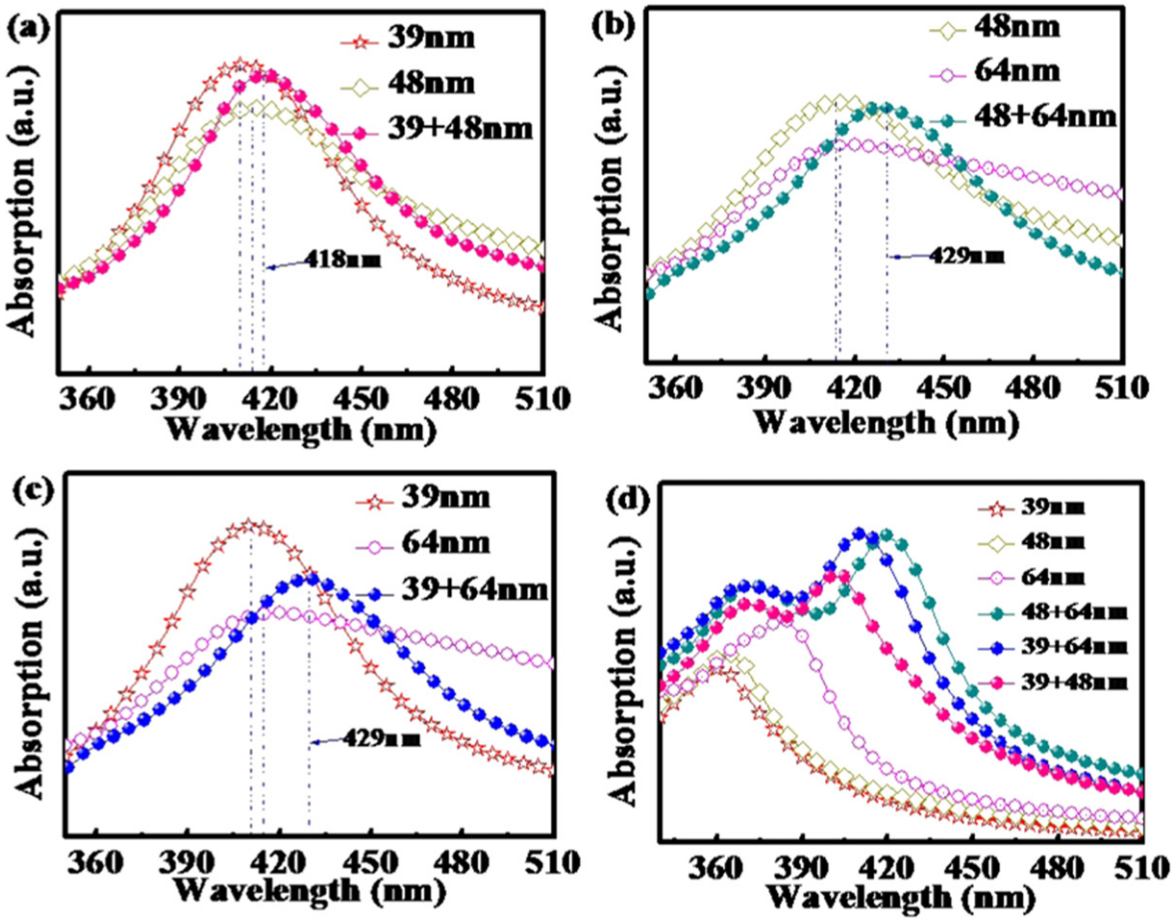

Figure 2. (a) Absorption spectra of Ag NPs (39 nm, 48 nm, 39 + 48 nm). (b) Absorption spectra of Ag NPs (48 nm, 64 nm, 48 + 64 nm). (c) Absorption spectra of Ag NPs (39 nm, 64 nm, 39 + 64 nm). (d) Simulated UV–vis absorption spectra of Ag NPs (39 nm, 48 nm, 64 nm, 39 + 48 nm, 48 + 64 nm and 39 + 64 nm).

LSPR band is slightly different from the theoretical simulation, which is due to their morphology difference. It is interesting to note that when the Ag NPs' size increases from 39 ± 2 nm to 64 ± 2.5 nm (figure 1(f)), an obvious red-shift from 411 to 419 nm will happen. Such size dependent LSPR peaks are due to the reduced coulomb force for relatively large particles, which is in harmony with previous studies [33, 34].

To study the effect of size distribution on the absorption spectrum, Ag NPs of different sizes were mixed in a volume ratio of 1:1. During analysis, three kinds of mixed samples which were obtained by mixing Ag NPs with 39 and 48 nm, 48 and 64 nm, 39 and 64 nm, respectively (figures 2(a)–(c)) were studied. It is observed that once mixed with Ag NPs of different sizes, the absorption peaks of all the three mixed samples will shift towards a longer wavelength in comparison with that of unmixed Ag NPs. FEM was then used to simulate the optical properties of Ag NPs in order to reveal the underlying reason behind the observed red-shift. It shows that there is an obvious red-shift of absorption peaks of Ag NPs when the size of Ag NPs increases from 39 to 64 nm, which is consistent with the results shown in figure 1. To understand the inter-particle coupling interaction of a random size distribution of Ag NPs, a model consisting of a central sphere and a surrounding sphere was built to calculate the absorption spectra. It can be seen that after blending different sized Ag NPs in a ratio of 1:1, the absorption peak of Ag NPs moves to a longer wavelength, which supports our experimental data very well (figure 2(d)). This finding is probably related to the break-down of the symmetry of plasmonic NPs, because the asymmetric type coupling interaction between NPs will lead to plasmon redistribution and shifting of the resonance peak position, which can highly tune the spectral position of the surface plasmon resonances [35–38]. Notably, there is only one peak in the experimental absorption spectrum, but for the simulated absorption spectrum of blending NPs, there are two strong peaks. Such a divergence can be understood as, unlike the pure Ag NPs without mixing, the experimental spectrum of mixed Ag NPs actually contains several superimposed spectra (more than two peaks). Considering that the absorption peaks of mixed Ag NPs are relatively close to the band gap of the ZnSe:Sb NRs (E_{gZnSe}:480 nm), mixed Ag NPs were used to decorate the optoelectronic devices.

Figure 3(a) shows the typical SEM images of as-synthesized ZnSe:Sb NRs. The ZnSe NRs are long ribbon-like nanostructures with a width of about 800 nm (the inset in figure 3(a)). The surfaces are clean and smooth without visible particles and impurities. What is more, the XRD

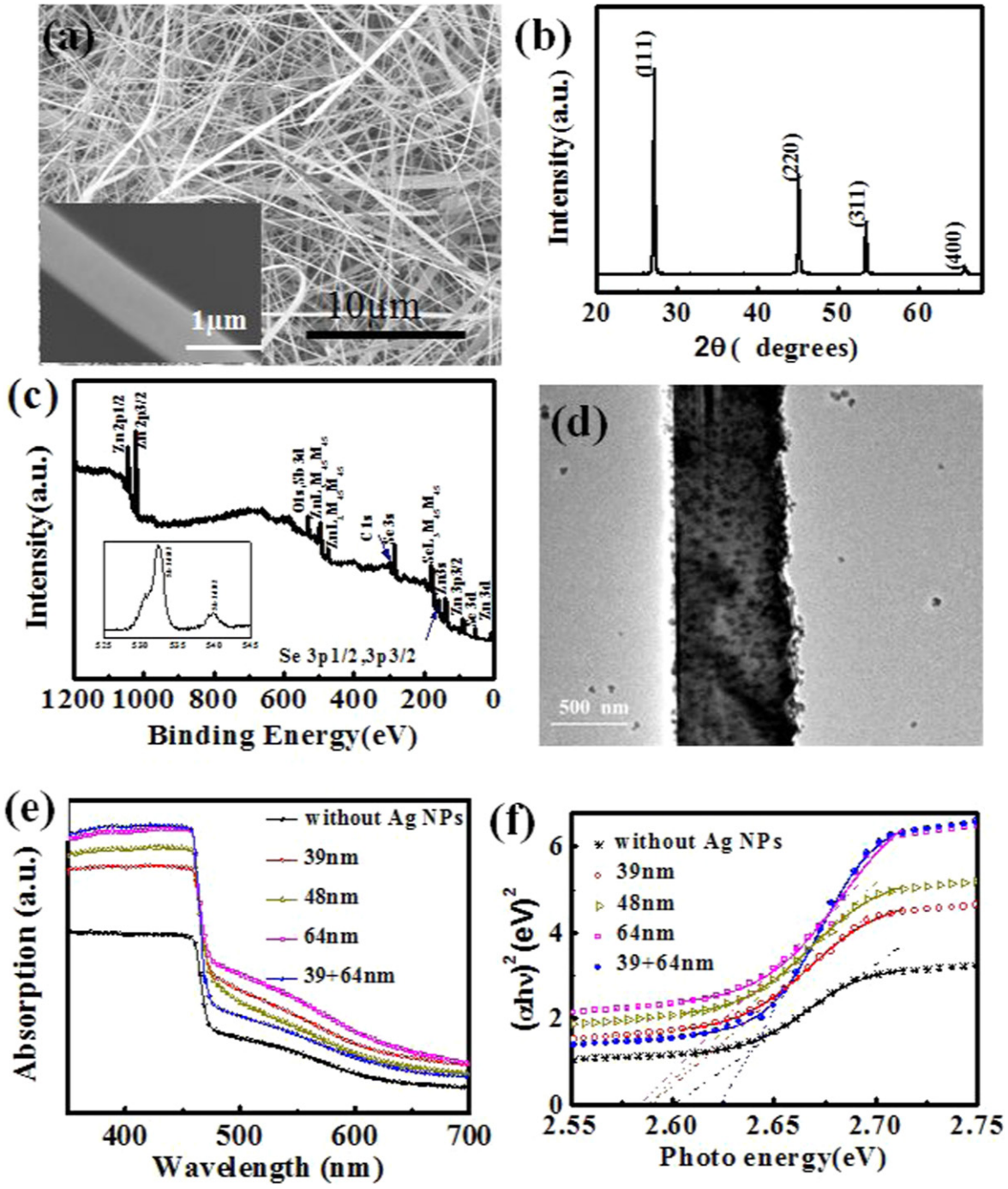

Figure 3. (a) SEM images of synthesized ZnSe:Sb NRs. (b) XRD pattern of the ZnSe:Sb NRs. (c) XPS spectrum of the ZnSe:Sb NRs. (d) TEM images of ZnSe:Sb NRs modified with Ag NPs. UV–visible absorption spectra (e) and plots of $(\alpha h\nu)^2$ versus photon energy (eV) (f) of ZnSe NRs modified with Ag NPs (39 nm, 48 nm, 64 nm, and 39 + 64 nm).

analysis reveals that only diffraction peaks due to cubic ZnSe (JCPDS 37-1463) were observed in the XRD pattern (figure 3(b)), suggesting a pure phase of the product. Figure 3(c) plots the XPS analysis result, from which one can see two weak peaks corresponding to Sb 3d5/2 and Sb 3d3/2 core level emissions, suggesting the presence of a trace amount of Sb in the ZnSe NRs and the *p*-type electric conductivity. Figure 3(d) shows the TEM image of ZnSe:Sb NR modified with Ag NPs. Due to their contrasting distinct differences, both the Ag NPs and NR can be easily distinguished. To explore the optical properties of the ZnSe NRs modified with Ag NPs, the UV–vis absorption spectra of both ZnSe:Sb NRs and Ag NPs@ the ZnSe:Sb nano-composite were investigated. As shown in figure 3(e), pure ZnSe:Sb NRs exhibit relatively weak absorption in the range from 350–700 nm. But, once modified with Ag NPs, the light absorption of the composite nanostructures will be considerably enhanced, especially in the range from 350–460 nm.

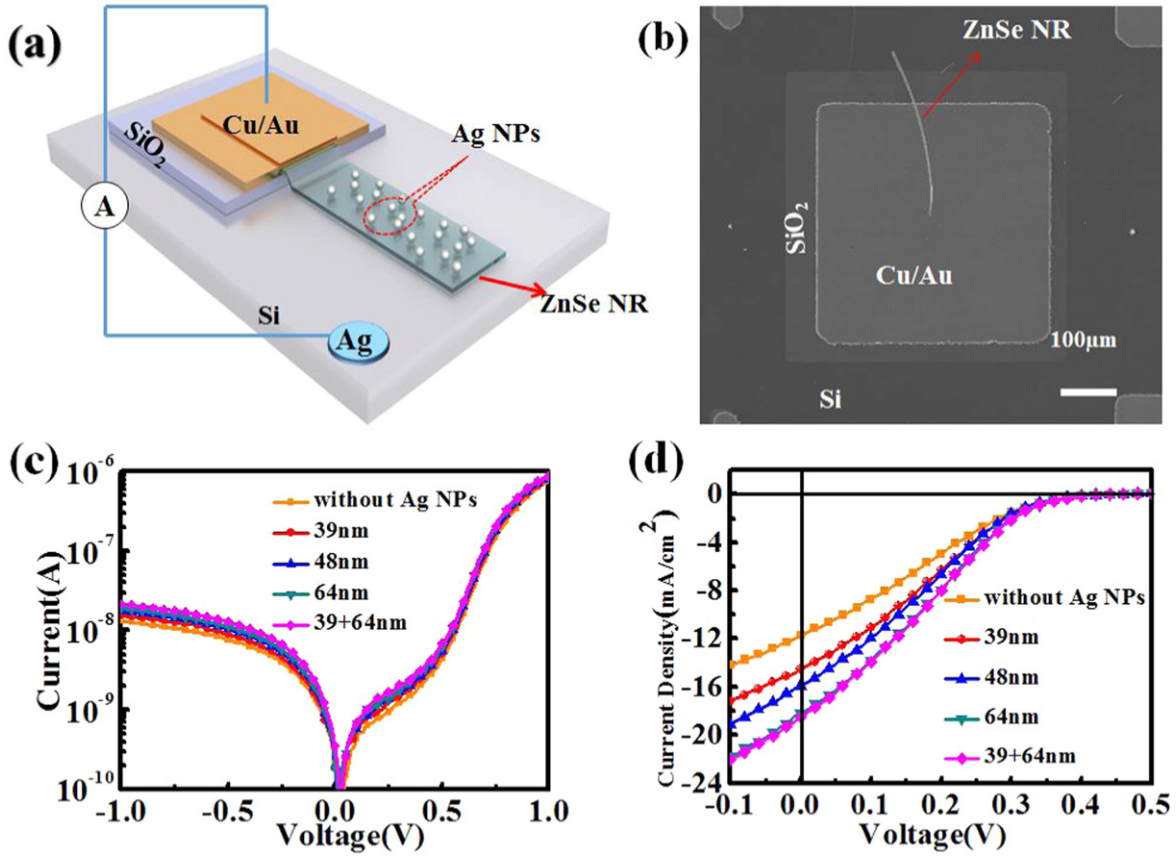

Figure 4. (a) Schematic illustration of ZnSe NR/Si heterojunction. (b) The top view SEM image of a single NR device. (c) Dark *I–V* characteristics of devices in the semi-logarithmic scale. (d) The *J–V* curves of devices embellished with different diameters of Ag NPs measured under AM 1.5 G illumination at 100 mW cm^{-2}.

Undoubtedly, such a light trapping effect induced by plasmonic Ag NPs is due to the longer effective light path lengths via multiple surface scatterings of the Ag NPs. In addition, it is interesting to find that with the increase of the Ag NPs' diameter, the light absorption of the Ag NPs@ZnSe:Sb NRs will become strong. This finding is understandable in that the absorption cross-section of the Ag NPs is proportional to the particle volume [39]. For a direct bandgap semiconductor, the optical absorption near the band edge can be described by the equation of $\alpha h\nu = A\,(h\nu - E_g)^{1/2}$, where α, ν, E_g, and A are the absorption coefficient, the light frequency, the band gap energy of the semiconductor, and a constant, respectively. Extrapolating the curve in figure 3(f) finds that the band-gaps of ZnSe NRs decrease from 2.60 eV (without Ag NPs) to 2.58 eV with ZnSe NRs modified with Ag NPs of 39 nm to 64 nm, but increase to 2.62 eV when modified with mixed Ag NPs (39 + 64 nm). This indicates that modifying Ag NPs with a suitable size can not only improve the absorption ability of ZnSe NRs but also decrease its bandgap to absorb more light by only changing the size of Ag NPs.

In order to take advantage of the LSPR effect, the plasmonic Ag NPs were modified onto a ZnSe:Sb NR/Si p-n heterojunction device (see the schematic illustration of the device in figure 4(a)). Figure 4(b) displays a typical SEM image of the plasmonic device based on a ZnSe NR/Si p-n heterojunction. The typical *I–V* characteristics of a ZnSe:Sb NR/Si *p-n* heterojunction with or without Ag NPs modification under dark conditions was shown in figure 4(c), from which one can see that all the devices exhibit obvious rectifying characteristics at the ZnSe NR/Si interfaces, with a rectifying ratio as high as 100 at ±1 V. Careful examination of the curves finds that the Ag NPs modification can slightly improve the current density of the device in forward bias. What is more, no significant change in the leakage current is observed after the incorporation of Ag NPs. For the device at −1 V bias, the dark background current achieved 13.1, 15.2, 17.7, 18.9, 21.4 nA for devices without Ag NPs and with 39, 48, 64 nm, mixed Ag NPs, respectively. When illuminated by AM 1.5G illumination, all the devices show typical photovoltaic characteristics. Among the five devices with and without Ag decoration, the ZnSe NR/Si heterojunction modified with 39 + 64 nm Ag NPs displays the highest current density (figure 3(d)).

Table 1 summarizes various photovoltaic parameters of the above five devices measured under AM 1.5G illumination (100 mW cm^{-2}), in which the I_{sc}, V_{oc}, *FF*, and η depicts the short-circuit current, open-circuit voltage, fill factor and efficiency, respectively. It can be found that the device performance of Ag NP-decorated devices is remarkably improved compared to the device without Ag NPs, which could be attributed to the enhanced light absorption and electric field strength of the ZnSe NRs modified with Ag NPs by LSPR

Table 1. Device performances of devices with Ag NPs and without Ag NPs.

Device	V_{oc} (V)	J_{sc}(mA cm^{-2})	FF(%)	η(%)
Without Ag NPs	0.46	11.75	19.29	1.04
39 nm	0.46	14.56	19.97	1.34
48 nm	0.44	15.90	20.35	1.42
64 nm	0.44	18.17	20.73	1.66
39 + 64 nm	0.44	18.52	20.66	1.68

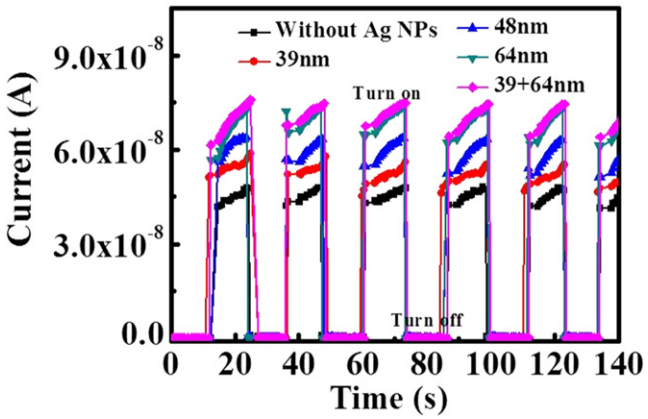

Figure 5. Time response spectra of the devices without and with decoration of 39, 48, 64, 39 + 64 nm Ag NPs measured at zero voltage bias.

effects, leading to more electron-hole pairs generation. The short-circuit current density increases from $J_{sc} = 11.75\,\text{mA cm}^{-2}$ for a device without Ag NPs to $18.17\,\text{mA cm}^{-2}$ for a Ag NP-decorated device when the size of Ag NPs increases to 64 nm. The current gain gives a rise of the conversion efficiency from $\eta = 1.04\%$ to 1.66%, while the fill factor increases from 19.29% to 20.73%. Very interestingly, a device decorated with mixed Ag NPs (39 + 64 nm) shows relatively better solar cell performance. Typically, its device parameters are estimated to be $V_{oc} = 0.44\,\text{V}$, $J_{sc} = 18.52\,\text{mA cm}^{-2}$, $FF = 20.66\%$, $\eta = 1.68\%$, respectively. This enhancement is related to the enhanced light absorption capability after modifying with mixed Ag NPs.

Figure 5 shows the photoresponse of pure ZnSe and ZnSe NRs decorated by Ag NPs when the light was turned on and off alternately at zero bias voltage. Obviously, the present device is highly sensitive to the light illumination, which signifies that the electron-hole pairs could be efficiently generated and separated in the ZnSe/Si heterojunctions. On the other hand, such photoresponse behavior is highly reversible and reproducible. To quantitatively evaluate the device performance, both responsivity (R) and detectivity (D^*) were calculated using the following equations:

$$R(AW^{-1}) = \left(\frac{I_p}{P_{opt}}\right) \tag{1}$$

Table 2. Summary of the key device parameters of the ZnSe:Sb NR/Si heterojunction.

Device	Responsivity (mA W^{-1})	Detectivity (cm Hz$^{1/2}$ W^{-1})	I_{on}/I_{off}
Without Ag NPs	117.2	5.86×10^{11}	0.94×10^3
39 nm	145.9	7.30×10^{11}	1.16×10^3
48 nm	158.6	7.90×10^{11}	1.27×10^3
64 nm	182.0	9.10×10^{11}	1.45×10^3
39 + 64 nm	184.8	9.20×10^{11}	1.48×10^3

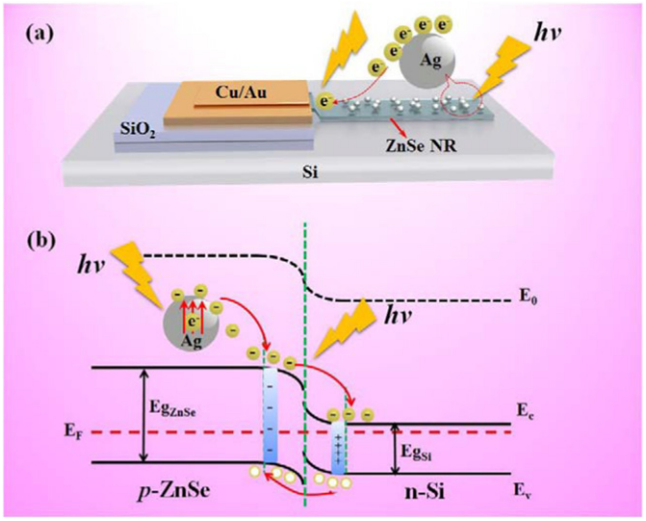

Figure 6. (a) Schematic illustration of LPSR excited electrons transfer from Ag NPs to ZnSe NRs. (b) Energy band diagram of ZnSe NR/Si heterojunction modified with Ag NPs under light illumination.

$$D^* = \frac{1}{NEP} \approx \sqrt{\frac{A}{2qI_d}}R. \tag{2}$$

where, I_p is the photocurrent, P_{opt} the incident light power, q the elementary charge (1.6×10^{-19} C), A the active area of the device and I_d the dark current, respectively. Based on the above equations, R was estimated to be $117.2\,\text{mA W}^{-1}$ for ZnSe NR without Ag NPs, $145.9\,\text{mA W}^{-1}$, $158.6\,\text{mA W}^{-1}$, $182.0\,\text{mA W}^{-1}$ and $184.8\,\text{mA W}^{-1}$ for ZnSe modificated with Ag NPs of 39 nm, 48 nm, 64 nm and 39 + 64 nm, respectively. Furthermore, the D^* was calculated to be $5.86 \times 10^{11}\,\text{cm Hz}^{1/2}\,\text{W}^{-1}$ for ZnSe NR without Ag NPs and 7.30×10^{11}, 7.90×10^{11}, 9.10×10^{11}, $9.20 \times 10^{11}\,\text{cm Hz}^{1/2}\,\text{W}^{-1}$ for devices modified by Ag NPs with a diameter of 39, 48, 64 and 39 + 64 nm, respectively. The key metrics of the present devices are briefly summarized in table 2. It clearly shows that the on-off ratio, R and D^* for the Ag NPs@ZnSe:Sb-Si devices are much higher than the device without Ag NPs. Additionally, the device decorated with mixed Ag NPs of both 39 and 64 nm has the highest photocurrent, which is in agreement with the previous optical property.

Figure 6 shows the schematic illustration of the device mechanism. A space charge region (or a built-in electric field)

was firstly formed at the ZnSe/Si heterojunction interface as a result of band bending from the Si substrate to ZnSe NRs due to their difference in work functions. When the light irradiates on the heterojunction, electron-hole pairs will be excited and then separated by the built-in electric field, giving rise to photovoltage and a photocurrent in the ZnSe NR/Si heterojunction. Notably, the generation of the photocurrent can be favorably enhanced when plasmonic Ag NPs are functionalized on the surface of the ZnSe NRs. The oscillating electrons (hot electrons) in the Ag NPs can be photo-excited to a high energy level, and can be transferred from the Ag NPs to the surface of the ZnSe NRs. This phenomenon has been reported in previous work, according to which the oscillating electrons in the Ag NPs can be readily transferred to the nearby II-VI nanostructures [40–42]. In this case, in addition to the general contribution of ZnSe: Sb NR/Si under light illumination, the photocurrent of the plasmonic optoelectronic device also enjoys the extra contribution from the plasmonic Ag NPs induced hot electron injection. As shown in figure 6(a), when the heterojunction was irradiated by light illumination, the energetic hot electrons from the LSPR excitation of metallic plasmonic NPs can easily transfer to the nearby ZnSe NR with a relatively high energy. The injected electrons at the ZnSe NRs could migrate to the ZnSe/Si heterojunction interface, and were then separated by the built-in electric field (figure 6(b)). As a consequence, the plasmonic device exhibits enhanced photocurrent in comparison with a device without Ag NPs. Note that in this study, the SPR peaks of Ag NPs can be readily tuned by tailoring the diameter of Ag NPs. This convenience allows us to develop a high performance optoelectronic device with very specific spectral selectivity.

Conclusion

To summarize, the efficiency of ZnSe NR/Si heterojunction optoelectronics was effectively enhanced by localized surface plasmon resonance of Ag NPs. Optical property analysis revealed that the absorption peak position of Ag NPs can be remarkably tuned by changing the size of Ag NPs. It was found that the modification of plasmonic Ag NPs with suitable sizes considerably increased the light absorption of the ZnSe NR/Si heterojunction. Further device analysis found that the short-circuit photocurrent density of the Ag NPs modified ZnSe NR/Si heterojunction solar cell was improved from 11.75 to 18.52 mA cm^{-2} compared to that without Ag nanopheres, with an enhancement up to 57.6%. In addition, the responsivity of the ZnSe NRs/Si heterojunction photodetector increased from 117.2 mA W^{-1} to 184.8 mA W^{-1} after modification with Ag nanospheres (39 + 64 nm), and its detectivity rose from 5.86×10^{11} cm $Hz^{1/2}$ W^{-1} to 9.20×10^{11} cm $Hz^{1/2}$ W^{-1}. The above result confirms that the plasmonic Ag NPs are good candidates for optimization of the optoelectronic devices.

Acknowledgments

We would like to thank Christina Souza of the University of Toronto for her useful advice about the analysis of optical data. This work was supported by the financial supports from Natural Science Foundation of China (Nos. NSFC Grant. 61575059), and the Fundamental Research Funds for the Central Universities (Nos.JZ2015HGXJ0182, 2013HGCH0012, 2014HGCH0005).

References

[1] Hagglund C, Zach M and Kasemo B 2008 *Appl. Phys. Lett.* **92** 013113
[2] Muller M B, Kuttner C, Konig T A F, Tsukruk V V, Stephan F, Karg M and Fery A 2014 *ACS Nano* **8** 9410
[3] Berini P, Olivieri A and Chen C K 2012 *Nanotechnology* **23** 444011
[4] Luo L B, Zeng L H, Xie C, Yu Y Q, Liang F X, Wu C Y, Wang L and Hu J G 2014 *Sci. Rep.* **4** 3914
[5] Wang Y, Ge C W, Zou Y F, Lu R, Zheng K, Zhang T F, Yu Y Q and Luo L B 2016 *Adv. Opt. Mater.* **4** 291
[6] Xu M, Feng J, Liu Y S, Jin Y, Wang H Y and Sun H B 2014 *Appl. Phys. Lett.* **105** 153303
[7] Jin Y, Feng J, Zhang X L, Xu M, Bi Y G, Chen Q D, Wang H Y and Sun H B 2012 *Appl. Phys. Lett.* **101** 163303
[8] Brabec C J, Sariciftci N S and Hummelen J C 2011 *Adv. Funct. Mater.* **11** 15
[9] Liu L, Stanchina W E and Li G 2009 *Appl. Phys. Lett.* **94** 233309
[10] Wang W L, Lin H, Li J B and Wang N 2008 *J. Am. Ceram. Soc.* **91** 628
[11] Nie B *et al* 2013 *Small* **9** 2872
[12] Jeon H C, Heo C J, Lee S Y and Yang S M 2012 *Adv. Funct. Mater.* **22** 4268
[13] Zhang Y J, Dong H L, Tang Q X, Ferdous S, Liu F, Mannsfeld S C B, Hu W P and Briseno A L 2010 *J. Am. Chem. Soc.* **132** 11580
[14] Li H X, Zhang Q L, Pan A L, Wang Y G, Zou B S and Fan H J 2011 *Chem. Mater.* **23** 1299
[15] Perng D C, Fang J F and Chen J W 2011 *J. Electrochem. Soc.* **158** H1097
[16] Dong H, Wu Z X, Lu F, Gao Y C, Ahmed E S, Jiao B, Ning S Y and Hou X 2014 *Nano Energy* **10** 181
[17] Luo L B, Xie W J, Zou Y F, Yu Y Q, Liang F X, Huang Z J and Zhou K Y 2015 *Opt. Express* **23** 12979
[18] Jain P K, Huang W Y and El S M A 2007 *Nano Lett.* **7** 2080
[19] Chan G H, Zhao J, Hicks E M, Schatz G C and Duyne R P V 2007 *Nano Lett.* **7** 1947
[20] Fong K E, Yung L and Yue L 2013 *Nanoscale* **5** 12043
[21] Morawiec S, Mendes M J, Mirabella S, Simone F, Priolo F and Crupi I 2013 *Nanotechnology* **24** 265601
[22] Zhang X L, Zhao J L, Wang S G, Dai H T and Sun X W 2014 *Int. J. Hydrogen Energy* **39** 8238
[23] Liu Y, Zhang X H, Jun S, Li H X, Zhang Q and Gao Y H 2014 *Opt. Express* **22** 030148
[24] Cho C Y, Kwon M K, Lee S J, Han S H, Kang J W, Kang S E, Lee D Y and Park S J 2010 *Nanotechnology* **21** 205201
[25] Zhu Z N, Liu W J, Li Z T, Han B, Zhou Y L, Gao Y and Tang Z Y 2012 *ACS Nano* **6** 2326
[26] Aćimović S S, Ortega M A, Sanz V, Berthelot J, Jose L G C, Renger J, Maerkl S J, Kreuzer M P and Quidant R 2014 *Nano Lett.* **14** 2636
[27] Lee S, Lee M H, Shin H J and Choi D 2013 *Nanotechnology* **24** 275702

[28] Hira T, Homma T, Uchiyama T, Kuwamura K and Saiki T 2013 *Appl. Phys. Lett.* **103** 241101
[29] Mulazimoglu E, Nogay G, Turan R and Unalan H E 2013 *Appl. Phys. Lett.* **103** 143124
[30] Battaglia C *et al* 2012 *ACS Nano* **6** 2790
[31] Tan H, Santbergen R, Smets A H M and Zeman M 2012 *Nano Lett.* **12** 4070
[32] Evanoff D D and Chumanov G 2005 *Chem. Phys. Chem.* **6** 1221
[33] Silvert P Y, Ronaldo H U and Kamar T E 1997 *J. Mater. Chem.* **7** 293
[34] Dongjo K, Sunho J and Jooho M 2006 *Nanotechnology* **17** 4019
[35] Jiang M M, Chen H Y, Li B H, Liu K W, Shan C X and Shen D Z 2014 *J. Mater. Chem.* C **2** 56
[36] Fan J A, Wu C, Bao K, Bao J, Bardhan R, Halas N J, Manoharan V N, Nordlander P, Shvets G and Capasso F 2010 *Science* **328** 1135
[37] Noguez C 2007 *J. Phys. Chem.* C **111** 3806
[38] West P R, Ishii S, Naik G V, Emani N K, Shalaev V M and Boltasseva A 2010 *Laser Photonics Rev.* **4** 795
[39] Luo L B, Huang X L, Wang M Z, Xie C, Wu C Y, Hu J G, Wang L and Huang J A 2014 *Small* **10** 2645
[40] Ni W H, An J, Lai C W, Ong H C and Xu J B 2006 *J. Appl. Phys.* **100** 026103
[41] Noh B Y, Baek S H, Jung Y I, Kim J H and Park I K 2013 *J. Nanosci. Nanotechnol.* **13** 3335
[42] Liu Y, Zhang X H, Su J, Li H X, Zhang Q and Gao Y H 2014 *Opt. Express* **22** 30148